Journal of Materials Chemistry A

RSC Publishing

PAPER

View Article Online
View Journal | View Issue

Cite this: J. Mater. Chem. A, 2013, 1, 4462

Indium-doped SnO_2 nanoparticle–graphene nanohybrids: simple one-pot synthesis and their selective detection of NO_2†

Shumao Cui,[a] Zhenhai Wen,[a] Eric C. Mattson,[b] Shun Mao,[a] Jingbo Chang,[a] Michael Weinert,[b] Carol J. Hirschmugl,[b] Marija Gajdardziska-Josifovska[b] and Junhong Chen*[a]

Received 28th December 2012
Accepted 12th February 2013

DOI: 10.1039/c3ta01673k

www.rsc.org/MaterialsA

We demonstrate novel nanohybrids of indium- and ruthenium-doped SnO_2 nanoparticles (NPs) on a reduced graphene oxide (RGO) surface prepared using a simple one-pot method at a relatively low temperature. The size of the doped SnO_2 NPs on the RGO is as small as 2–3 nm with uniform distribution. We find that the introduction of dopants facilitates the NP nucleation on graphene oxide. The gas sensing responses of the resulting nanohybrids demonstrate that the addition of indium in SnO_2 significantly enhances the sensitivity to NO_2 compared with RGO–SnO_2. The sensor also shows excellent selectivity to NO_2 when other common gases such as NH_3, H_2, CO and H_2S, are present. The sensing mechanism responsible for the superior sensitivity and selectivity of the nanohybrids is also discussed.

Introduction

Nanohybrids have been widely studied for various applications due to their enhanced mechanical, electrical, and optical properties.[1–5] Recently, graphene (G) and its chemically modified forms (*e.g.*, graphene oxide) have attracted extensive attention as a nanohybrid building block because of its unique mechanical, physical, and chemical properties.[6–11] For example, graphene has high mechanical strength (>1060 GPa), high thermal conductivity (~3000 W m^{-1} K^{-1}), high electron mobility (15 000 cm^2 V^{-1} s^{-1}), and a high specific surface area (2600 m^2 g^{-1}).[6–9] Graphene-based nanohybrids have been studied for various applications, including energy storage,[12–14] catalysis,[15,16] drug delivery,[17] and sensors.[18,19] Graphene is an especially promising gas sensing material because of its high electron mobility and high specific surface area. Various graphene–nanoparticle nanohybrids, including G–Pd, G–Pt, G–SnO_2, and G–ZnO_2, have been used in sensing applications.[19–22] These nanohybrids are usually synthesized either by *in situ* nanoparticle (NP) growth on graphene in solution or by directly mixing two previously prepared materials. However, the sensing application of graphene-based nanohybrids is still in its infancy.

Tin oxide (SnO_2) is a semiconducting inorganic material with a wide band gap of 3.62 eV at 298 K, which has been widely used for sensing applications.[23–25] To achieve high sensitivity and selectivity, both doping and shrinking the size of the nanocrystals of SnO_2 have been used.[26,27] It is expected that doping SnO_2 can be an efficient way to improve sensing performance for the following reasons: (1) the charge carrier concentration of semiconducting SnO_2 can be dramatically increased by dopants,[28,29] which may facilitate the electron transfer during the interaction with gases; (2) dopants can constrain the growth of SnO_2 crystals, forming very fine NPs in hydrothermal methods,[30] which will result in a high surface-to-volume ratio of SnO_2 NPs that are conducive for gas sensing applications; (3) a large amount of oxygen vacancies and chemisorbed oxygen species are generated by metal dopants,[31] and can lead to enhanced sensing response; and (4) the sensor selectivity toward a specific gas can be greatly improved by carefully choosing the dopant. For example, the selectivity to ethanol was enhanced by doping ceria in SnO_2,[32] and palladium-doped SnO_2 was designed to enhance the sensing selectivity to CH_4 and H_2.[33] However, those materials work only at elevated temperatures.

Nitrogen dioxide is a toxic gas produced by combustion in power plants and automobiles that can harm human health and the environment by causing acid rain.[34] It has been recommended that the exposure time to 3 ppm NO_2 be no longer than 8 h.[35] However, it is still a challenge to develop efficient sensors to selectively detect low concentrations of NO_2 at room temperature. Indium (In) and ruthenium (Ru) are commonly used as dopants in SnO_2 for sensing applications. They have been demonstrated to not only improve sensing properties toward NO_2 but also to lower the operating temperature.[36,37]

[a]Department of Mechanical Engineering, University of Wisconsin-Milwaukee, 3200 North Cramer Street, Milwaukee, WI 53211, USA. E-mail: jhchen@uwm.edu; Fax: +1-414-229-6958; Tel: +1-414-229-2615

[b]Department of Physics and Laboratory for Surface Studies, University of Wisconsin-Milwaukee, 1900 E. Kenwood Blvd, Milwaukee, WI, 53211, USA

† Electronic supplementary information (ESI) available. See DOI: 10.1039/c3ta01673k

In this work, we report on a one-pot strategy to achieve facile and low-cost fabrication of a unique nanohybrid, in which In-doped SnO_2 (IDTO) NPs uniformly distribute on reduced graphene oxide (RGO). We investigated the crystal growth mechanism and found that dopants facilitated the nucleation of SnO_2 crystals on graphene oxide (GO) surface. This method also can be used to fabricate SnO_2 NPs doped with other elements (*e.g.*, Ru) on RGO, and potentially can be used to synthesize other doped metal oxide (*e.g.*, TiO_2) or metal oxide nanocomposites on graphene. The Ru-doped SnO_2 NPs–RGO hybrids were also synthesized using the same method, and the control experiments further proved the role of dopants in the NP formation. The enhanced sensing performance of RGO/In-SnO_2 (RGO–IDTO) toward NO_2 was demonstrated at room temperature, reaching a detection limit as low as 0.3 ppm. Moreover, excellent selectivity was also achieved, as verified by testing several other gases with the same device. The tiny NPs offer a large number of active sites for gas adsorption, and the dopants play a critical role in enhancing sensor performance with RGO acting as a conducting channel.

Experimental

Synthesis

GO was prepared by oxidizing graphite powder (Bay Carbon, SP-1 graphite) under acidic conditions according to the modified Hummers method.[38] In a typical process to prepare RGO–IDTO, 8 mg GO was dispersed in 20 ml deionized water, and sonicated for 30 min. Then 0.5 ml $InCl_3$ (0.05 M) aqueous solution and 2.5 ml $SnCl_4$ (0.01 M) were added to the GO dispersion in sequence with magnetic stirring (400 rpm). The mixture was sonicated for 10 min to allow for uniform ion adsorption on the GO surface. After that, 15 ml $NaBH_4$ aqueous solution (30 mg per 10 ml) was added drop-wise into the above solution with stirring. Finally, the entire solution was kept at 50 °C on a hotplate for 1 h. The final product was collected by centrifuge. Ru-doped SnO_2 NPs decorated RGO (RGO–RDTO) were also prepared using the same method; 1 ml $RuCl_3$ (0.05 M) was used as the dopant source, and all the other chemicals and procedures were the same as those used for the RGO–IDTO synthesis.

Characterization

The samples were characterized using a number of techniques. The crystallographic structure of as-produced nanohybrids was investigated by X-ray diffraction (XRD). Scanning electron microscopy (SEM) was carried out with a Hitachi S-4800 electron microscope at an acceleration voltage of 10 kV. The structure of as-produced nanohybrids was characterized by transmission electron microscopy (TEM) (Hitachi H-9000-NAR). High-resolution TEM (HRTEM) and selected area electron diffraction (SAED) (at an acceleration voltage of 300 kV) were used to characterize the crystal structure of the nanohybrids. Energy dispersive X-ray spectroscopy (EDS Noran Si:Li detector) was used to characterize the elemental composition. The surface chemical composition was characterized by using X-ray photoelectron spectroscopy (XPS) (HP 5950A). Raman spectra were taken using a Raman spectrometer (Renishaw 1000B).

Gas sensor fabrication and sensing test

To prepare gas sensors composed of RGO–IDTO nanohybrids, gold interdigitated electrodes with finger width and inter-finger spacing of 2 μm and thickness of 50 nm were fabricated by an e-beam lithography process on a silicon wafer with a top SiO_2 layer of about 200 nm. The RGO–IDTO nanohybrids were dispersed in *N*,*N*-dimethylformamide (DMF), and then a drop (0.1 μl) of the dispersion was cast onto the gold electrode. Low concentration dispersion was used to avoid overlapping RGO sheets. To purify the sensor and improve the electrical contact between the nanohybrids and the gold electrodes, the sensor devices were annealed in a tube furnace at 200 °C for 1 h before sensing tests.

The gas sensing properties were tested in an air-tight chamber with electrical feedthroughs. A constant voltage was applied to the electrode gap bridged by the nanohybrids. Then the target gas with certified concentrations was flowed into the chamber, and the change in the current passing through the nanohybrids was monitored and recorded using a Keithley 2602 source meter (Keithley, Cleveland, OH). A typical sensing test cycle consisted of three sequential steps. First, a dry air flow was introduced into the sensing test chamber to record a baseline. Then, a target gas diluted in air was injected to register sensor signals. Finally, the sensor was recovered in a dry air flow. All the flow rates were controlled at 2 l min^{-1}, and the target gases were diluted in dry air. The sensor sensitivity was defined as $S = \Delta G/G_0$, where ΔG is the change in the sensor conductance before and after the gas exposure and G_0 is the sensor conductance in dry air. The resistance of RGO–IDTO nanohybrids was ~2 kΩ (or $G_0 = 0.0005$ S) in dry air before target gas exposure.

Results and discussion

Scheme 1 illustrates the preparation procedure of RGO–IDTO nanohybrids. First, indium ions were introduced into the GO dispersion by adding an $InCl_3$ aqueous solution under magnetic stirring. Then, tin ions were slowly added into the above mixture using $SnCl_4$ aqueous solution as the source. After sonication, a $NaBH_4$ solution was slowly dropped into the solution mixture to reduce GO. The obtained solution was then continuously stirred at 50 °C for 1 h and RGO–IDTO nanohybrids were obtained after centrifuging and washing.

The morphology of as-produced RGO–IDTO nanohybrids was first examined by a field-emission SEM. An overview of the RGO–IDTO nanohybrids is shown in Fig. S1,† which clearly indicates

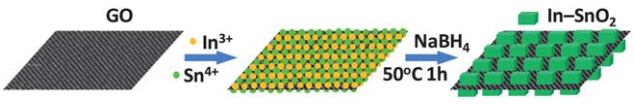

Scheme 1 Schematic illustration for the preparation process of RGO–IDTO nanohybrids.

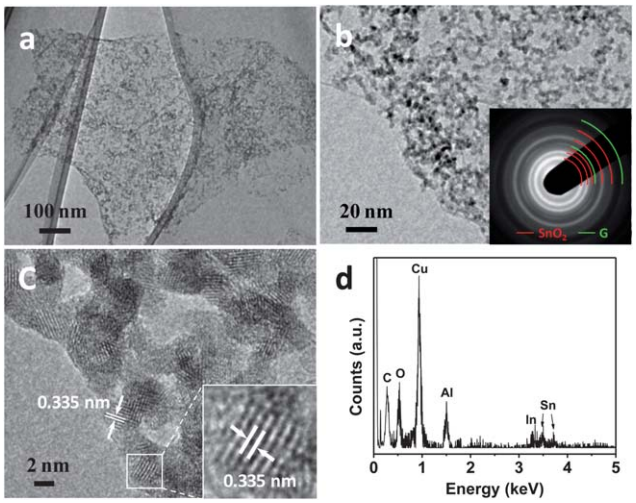

Fig. 1 (a and b) TEM images of RGO–IDTO nanohybrids. The inset in image (b) is the SAED pattern of RGO–IDTO. The rings marked with red arcs are indexed to rutile SnO_2, and the rings marked with green arc are indexed to graphene. (c) HRTEM image of RGO–IDTO nanohybrids. (d) EDS spectra of RGO–IDTO. Cu and Al are from the sample holder.

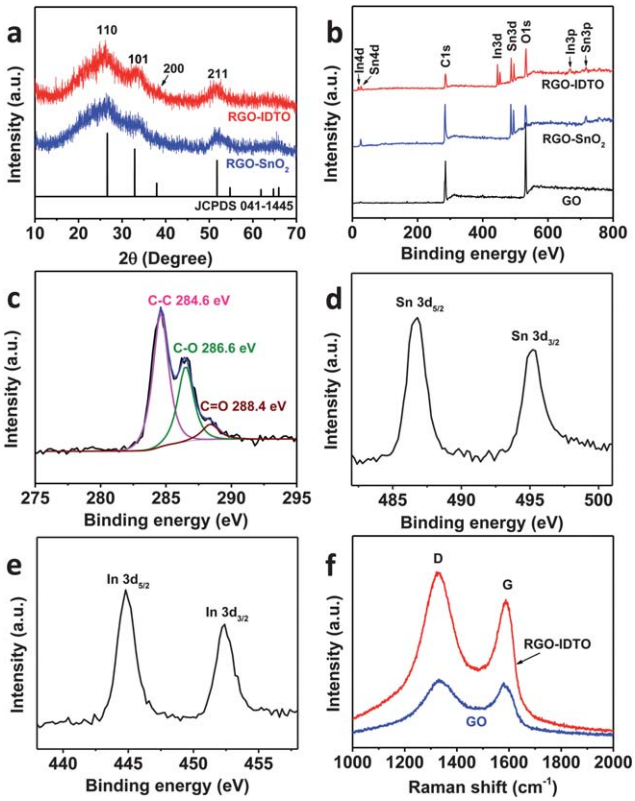

Fig. 2 (a) XRD patterns of RGO–SnO_2 and RGO–IDTO nanohybrids. (b) XPS spectra of GO, RGO–SnO_2, and RGO–IDTO nanohybrids. (c–e) High-resolution XPS spectra of C 1s (c), Sn 3d (d), and In 3d (e) of the RGO–IDTO nanohybrids. (f) Raman spectra of GO and RGO–IDTO nanohybrids.

that the nanohybrids retain the sheet structure typical for graphene. The nanostructure was further investigated using TEM (Fig. 1a), showing that the IDTO nanostructures are uniformly coated on the RGO sheet. A typical magnified TEM image is shown in Fig. 1b, demonstrating that a thin lacy network of IDTO NPs is uniformly distributed on the surface of graphene. The inset of Fig. 1b is the SAED pattern of RGO–IDTO with well-defined rings composed of two parts. The rings marked with red arcs (from the inside to outside) are indexed to rutile SnO_2 (110), (101), (200), (211), and (112) planes. Meanwhile, the rings marked with green arcs (from the inside to outside) are indexed to {100}- and {110}-type reflections of graphene, consistent with graphene and with the known structure of RGO with disordered oxygen functional groups. The IDTO nanocrystals anchored on the RGO sheets were further analyzed using HRTEM. As shown in Fig. 1c, IDTO nanocrystals with clear lattice fringes are observed with sizes of about 2–3 nm. The labeled lattice spacing of 0.335 nm corresponds with the unique (110) plane of rutile SnO_2. To examine the elemental composition of NPs, EDS was performed and the result indicates that there is indium in the nanohybrid. Similar results were obtained for RGO–RDTO nanohybrids, as shown in Fig. S2.† For substitutional doping, the difference in ionic radii should be less than the Hume-Rothery limit (15%).[39] The ionic sizes of Sn^{4+}, In^{3+}, and Ru^{4+} are 0.083 nm, 0.081 nm, and 0.076 nm, respectively,[40,41] with a maximum difference of 8.4%, which lies within the Hume-Rothery limit. Thus, when In and Ru are doped in SnO_2, In^{3+} and Ru^{4+} can substitute for Sn^{4+}, forming a uniformly stable solid solution, consistent with previous reports.[41,42]

To obtain information about the average crystallographic structure, the RGO–IDTO nanohybrid was characterized using XRD (Fig. 2a). For comparison, RGO–SnO_2 without dopants was synthesized using a two-step method published previously.[43] Briefly, Sn^{4+} was introduced into the GO dispersion and adsorbed on the surface of GO bonded with oxygen functional groups (*e.g.*, hydroxyl and carbonyl groups) by electrostatic force. Then the precipitate was collected and washed with centrifugation. The product was dried at 80 °C overnight, and RGO–SnO_2 was obtained after annealing treatment at 350 °C for 2 h under argon atmosphere. The XRD pattern in Fig. 2a demonstrates the presence of crystalline IDTO NPs through the diffraction peaks corresponding with the (110), (101), (200), and (211) planes of rutile SnO_2 (JCPDS 041-1445). The broad peaks indicate that the nanocrystals are tiny, consistent with TEM results. There are no other peaks except for one weak peak around 25.5° corresponding to the (002) plane of few-layer RGO, suggesting that pure IDTO NPs are anchored on the surface of RGO during the synthesis. The XRD pattern of RGO–IDTO is very similar to that of RGO–SnO_2, suggesting that there were no phase changes occurring and no nanoscale separation with indium doping in SnO_2, which is consistent with the previous report.[29] The above results suggest that the dopant ions are homogenously distributed in the SnO_2 lattice. The XRD pattern of RGO–RDTO shows similar characteristics (Fig. S3†).

The surface composition of RGO–IDTO was characterized by XPS. Fig. 2b shows the entire survey spectra of RGO–IDTO, showing the existence of C, O, In, and Sn in the nanohybrid, consistent with the EDS results. The C/O ratios were 1.8 for the initial GO and 1.6 for RGO–IDTO hybrids based on the XPS analysis. Although our electrical measurements presented later suggest that GO has been effectively reduced to RGO during the synthesis process, it is quite challenging to determine the exact

degree of reduction of GO because the oxygen signal in the XPS is from both RGO and IDTO. Fig. 2c–e show high-resolution XPS spectra of C 1s, Sn 3d, and In 3d, respectively. The complex C 1s XPS spectra can be fitted to three components with peaks centered at 284.6, 286.6, and 288.4 eV, corresponding with C–C, C–O, and C(O)O, respectively. The binding energies of C–O and C(O)O indicate the existence of oxygen groups in RGO.[19] Fig. 2d presents the Sn 3d level from IDTO, showing two symmetric peaks due to spin–orbit splitting with binding energies of 495.2 and 486.8 eV for the $d_{3/2}$ and $d_{5/2}$ lines, respectively. Similarly, the In 3d level (Fig. 2e) consists of two peaks centered at 452.4 and 444.8 eV for the $d_{3/2}$ and $d_{5/2}$ lines, respectively. The as-produced RGO–IDTO nanohybrid was also investigated by Raman spectroscopy (Fig. 2f). The peak at about 1587 cm^{-1} (G band) corresponds to the in-plane vibration of sp^2 carbon–carbon bonds while the peak at about 1330 cm^{-1} (D band) is attributed to disorders and defects of the graphitic layer.[44] The D/G intensity ratio (I_D/I_G) indicates the extent of π-conjugation and the defect density in the graphitic layer.[45] The increase of I_D/I_G for RGO–IDTO (1.16) compared with that of GO (1.04) suggests a decrease in the average size of sp^2 domains and a high concentration of defects, possibly caused by the sonication and reduction process. This increase in I_D/I_G also agrees with other reported results.[46,47]

Based on our experiments, we believe that the dopant In plays a critical role in the nucleation of the doped tin oxide. For example, when only Sn and GO (no In) were used in the reaction system with the same experimental procedure, the resulting product consisted of aggregated NPs partially covering the RGO surface (Fig. S4a†). The SAED pattern in Fig. S4b† demonstrates that the NPs on RGO have poor crystalline structure, as evidenced by the broad blurry rings. When using In, the time when In is added is important, affecting the final NP dispersion and crystallization. It was found that similar well-defined RGO–IDTO nanohybrid products were obtained when mixing the two ion sources and then adding them into the GO dispersion, as well as when adding In first followed by adding Sn using the same molar ratio of In/Sn = 1 : 1 (Fig. 1, S5a and b†). However, when adding Sn before In, the results were similar to those obtained when adding Sn only into the GO dispersion (Fig. S6†). A possible reason is that Sn adsorbs on the GO surface, occupying most of the available ion adsorption sites on the GO surface. Therefore, limited sites are left for In adsorption, resulting in the poor nanoparticle crystallization and dispersion.

Both the presence and the amount of dopant ions play a critical role in the formation of IDTO NPs on the GO surface. To investigate the effect of In on the final product, different amounts of In were used in the synthesis of IDTO NPs while keeping the same amount of Sn, *i.e.*, molar ratios of In/Sn = 1 : 1, 0.5 : 1, and 0.3 : 1. The as-produced nanohybrids were characterized by TEM and SAED, shown in Fig. S5.† It was found that the samples with the largest amount of In (In/Sn = 1 : 1) produced the best crystalline IDTO NPs on the RGO surface (Fig. S5a and b†), as evidenced by the clear nanoparticle distinction and bright sharp SAED rings. The sample synthesized with the smallest amount of In (In/Sn = 0.3 : 1) produced NPs over the RGO surface with broad diffraction rings (Fig. S5e and f†), indicating poor crystallization of IDTO nanoparticles. Therefore, it is reasonable to conclude that In can lower the nucleation energy of NPs, which means that well-defined IDTO nanocrystals would easily form on the GO surface with a higher concentration of In. We also investigated the function of Ru in the nucleation of RDTO NPs, and found that fine crystalline NPs formed on the RGO when Ru is introduced before adding Sn into the GO dispersion. With the increase of Ru in the solution, a higher density of RDTO nanoparticles formed on the RGO surface (Fig. S7†). Because the dopants encourage the final evenly distributed crystalline NPs on graphene, we propose that the IDTO/RDTO nanocrystals form at positions where dopant ions are located on the GO surface with low nucleation energy at a low temperature.

Our previous study showed that SnO_2 nanocrystals enhance the sensing sensitivity of RGO to NO_2.[19] To prove dopants can further improve the sensing performance, we investigated the sensing properties of RGO–IDTO to NO_2 at room temperature. The dynamic sensing performance of the sensor was measured under different NO_2 concentrations (Fig. 3a and b). The electrical conductivity of the hybrid sensor increases upon exposure to NO_2, which is consistent with our previous results for RGO–SnO_2 sensors. Because NO_2 is an oxidizing gas, when NO_2 is adsorbed on SnO_2 surface, we proposed that there is electron transfer from SnO_2 to NO_2.[4,19] The RGO usually behaves as a p-type semiconductor in air at room temperature and was used as a conducting channel in our device.[38] The electron transfer effectively increases the charge carrier (*i.e.*, hole) concentration in RGO, leading to an increase in electrical conductivity. The results also demonstrate that RGO–IDTO nanohybrids show p-type semiconducting behavior, and the semiconducting type of the RGO was not changed after the IDTO NP decoration.

The sensitivity of the sensor decreases upon exposure to lower concentrations of NO_2. For the NO_2 concentrations investigated (from 0.3 to 100 ppm), the sensing response can be

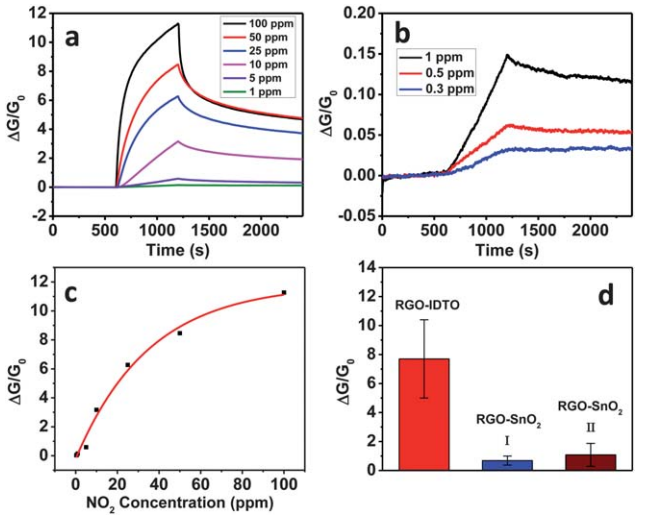

Fig. 3 (a and b) Dynamic sensing response of RGO–IDTO toward different NO_2 concentrations. (c) Exponential curve of sensitivity as a function of NO_2 concentration. (d) Sensitivity comparison of RGO–IDTO and RGO–SnO_2 nanohybrids to 100 ppm NO_2.

fitted well by an exponential curve, as shown in Fig. 3c. For low concentration detection, the sensor can respond to a concentration level as low as 0.3 ppm, as shown in Fig. 3b, which is an order of magnitude lower than the EPA recommended exposure limit (3 ppm).[35] Our sensor thus could be used for room-temperature low concentration NO_2 detection. The recovery process of the sensor, however, is slow, taking overnight to completely recover to the initial state. Further sensor optimization is needed to shorten the recovery time.

To prove the sensing enhancement of dopants to NO_2, the sensitivities were compared for two types of RGO–SnO_2 hybrids fabricated using two different methods. The first series of samples (RGO–SnO_2 I) were synthesized using the hydrothermal method described above.[43] The second series of samples (RGO–SnO_2 II) were synthesized by loading SnO_2 NPs on RGO using a mini-arc plasma source.[19] The sensitivity of the RGO–IDTO nanohybrids is much higher than that of RGO–SnO_2 (Fig. 3d), indicating that In doping in SnO_2 NPs can greatly enhance the sensitivity. This result can be attributed to the increase of oxygen species (*e.g.*, $O^{\delta-}$ adsorbates) on the nanoparticle surface by introducing indium as a dopant. As investigated by density functional theory (DFT) calculations, the interaction between the SnO_2 surface and NO_2 molecules can be described as follows: NO_2 (gas) + $O^{\delta-} = NO_3^{\delta-}$ (adsorption), where NO_2 is attached to $O^{\delta-}$ on the SnO_2 surface, forming a $NO_3^{\delta-}$ complex, with electron transfer occurring from the nanoparticle to NO_2.[48] A higher sensitivity suggests more NO_2 molecular adsorption and more electron transfer from the NPs to NO_2. Moreover, it has been found that dopants in SnO_2 increase the number of oxygen vacancies,[31] which in turn can easily dissociate oxygen molecules and thus form chemisorbed oxygen species.[49] Since our samples were exposed to air before testing, oxygen in the air might be dissociated and chemisorbed on the IDTO surface. This is also consistent with other observations that the dopant facilitates adsorption of oxygen molecules and formation of oxygen ions on the SnO_2 surface.[50] The high sensitivity might also be attributed to the tiny size of IDTO nanocrystals due to their large surface-to-volume ratio, which leads to ample adsorption sites in the sensing process and thus an enhanced sensitivity. For NO_2 detection, other efficient graphene-based hybrid sensors have also been reported, such as G–WO_3 and RGO–Cu_2O sensors.[51,52] Our RGO–IDTO sensors reported here have a comparable lower detection limit with RGO–Cu_2O sensors, which are better than G–WO_3 sensors. However, there was no report on the selectivity of those nanohybrids.

In order to probe the selectivity of RGO–IDTO nanohybrid sensors, the same sensor was measured against several other gases, including H_2S, CO, H_2, and NH_3. The sensing test cycle was the same as that for measuring NO_2, and the dynamic responses are shown in Fig. 4a. The sensor showed very weak response to all gases except NO_2. The device conductance decreased when the sensor was exposed to NH_3, indicating electron transfer from NH_3 to the nanohybrids. However, the exposure to other gases led to an increase of the conductance, suggesting the electron transfer is in the opposite direction, *i.e.*, from the nanohybrids to the gas molecules. The sensitivity comparison shown in Fig. 4b demonstrates that the response to other testing gases is

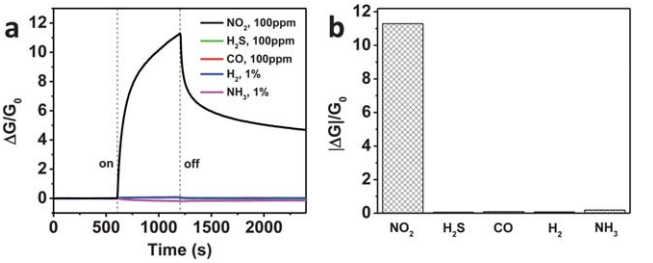

Fig. 4 Comparison of sensing responses (a) and sensitivity (b) to various gases.

negligible compared with that of NO_2, indicating that our sensor has very good selectivity. Here, we suggest a "superposition effect" as one possible mechanism for the high selectivity: our previous experimental and theoretical studies showed that SnO_2 selectively enhanced the sensitivity of MWCNTs or RGO to NO_2 at room temperature.[19,48] It was also reported that multiple In_2O_3 nanowire can achieve selective detection of NO_2 with other chemical gases such as NH_3, O_2, CO, and H_2.[53] Therefore, the differential selectivity of the RGO–IDTO hybrids was maximized by doping indium in SnO_2 for this study due to the same gas selectivity enhancement. However, more work is needed to better understand the underlying mechanism.

Conclusions

In summary, RGO–IDTO and RGO–RDTO nanohybrids were successfully synthesized using a simple one-pot aqueous method at low temperature. The morphology characterization results show that In- and Ru-doped SnO_2 NPs are evenly distributed on the RGO surface, and that the dopants are successfully incorporated into the SnO_2 nanocrystals. The size of the doped nanoparticles is very small, about 2–3 nm. The dopants lower the nucleation energy of the ions on GO and lead to crystalline IDTO or RDTO NPs on the RGO surface. Such nanohybrids are very promising for sensitive and selective detection of NO_2. The as-prepared RGO–IDTO showed a much higher sensitivity than RGO–SnO_2, indicating the sensing enhancement function of indium doping. The dopants also induced a large number of oxygen vacancies in the nanocrystals, leading to an increase in the number of surface oxygen ion species that can react with NO_2 gas molecules. The highly selective sensing to NO_2 can be understood as a "superposition effect" of selectivity in the hybrids. This preparation method opens up a simple one-pot approach to synthesize various metal-doped metal oxide nanoparticle–graphene nanohybrids for a wide range of applications such as sensors and catalysis.

Acknowledgements

The authors acknowledge financial support from the National Science Foundation (CMMI-0900509), and from the Research Growth Initiative Program of the University of Wisconsin-Milwaukee (UWM). The SEM imaging was conducted at the UWM Bioscience Electron Microscope Facility, and TEM analyses were conducted in the UWM Physics HRTEM Laboratory. Sensor

electrodes were fabricated at CNM of Argonne National Laboratory, supported by U.S. DOE (DE-AC02-06CH11357).

References

1 A. C. Balazs, T. Emrick and T. P. Russell, *Science*, 2006, **314**, 1107.
2 L. L. Beecroft and C. K. Ober, *Chem. Mater.*, 1997, **9**, 1302.
3 H. Y. Fan, K. Yang, D. M. Boye, T. Sigmon, K. J. Malloy, H. F. Xu, G. P. Lopez and C. J. Brinker, *Science*, 2004, **304**, 567.
4 G. H. Lu, L. E. Ocola and J. H. Chen, *Adv. Mater.*, 2009, **21**, 2487.
5 A. L. M. Reddy, M. M. Shaijumon, S. R. Gowda and P. M. Ajayan, *Nano Lett.*, 2009, **9**, 1002.
6 A. K. Geim and K. S. Novoselov, *Nat. Mater.*, 2007, **6**, 183.
7 A. H. Castro Neto, F. Guinea, N. M. R. Peres, K. S. Novoselov and A. K. Geim, *Rev. Mod. Phys.*, 2009, **81**, 109.
8 K. S. Novoselov, A. K. Geim, S. V. Morozov, D. Jiang, Y. Zhang, S. V. Dubonos, I. V. Grigorieva and A. A. Firsov, *Science*, 2004, **306**, 666.
9 D. R. Dreyer, R. S. Ruoff and C. W. Bielawski, *Angew. Chem., Int. Ed.*, 2010, **49**, 9336.
10 D. R. Dreyer, S. Park, C. W. Bielawski and R. S. Ruoff, *Chem. Soc. Rev.*, 2010, **39**, 228.
11 S. H. Lee, H. W. Kim, J. O. Hwang, W. J. Lee, J. Kwon, C. W. Bielawski, R. S. Ruoff and S. O. Kim, *Angew. Chem., Int. Ed.*, 2010, **49**, 10084.
12 D. H. Wang, R. Kou, D. Choi, Z. G. Yang, Z. M. Nie, J. Li, L. V. Saraf, D. H. Hu, J. G. Zhang, G. L. Graff, J. Liu, M. A. Pope and I. A. Aksay, *ACS Nano*, 2010, **4**, 1587.
13 A. L. M. Reddy, A. Srivastava, S. R. Gowda, H. Gullapalli, M. Dubey and P. M. Ajayan, *ACS Nano*, 2010, **4**, 6337.
14 J. R. Potts, D. R. Dreyer, C. W. Bielawski and R. S. Ruoff, *Polymer*, 2011, **52**, 5.
15 H. Zhang, X. J. Lv, Y. M. Li, Y. Wang and J. H. Li, *ACS Nano*, 2010, **4**, 380.
16 I. V. Lightcap, T. H. Kosel and P. V. Kamat, *Nano Lett.*, 2010, **10**, 577.
17 X. Y. Yang, X. Y. Zhang, Y. F. Ma, Y. Huang, Y. S. Wang and Y. S. Chen, *J. Mater. Chem.*, 2009, **19**, 2710.
18 M. Shafiei, P. G. Spizzirri, R. Arsat, J. Yu, J. du Plessis, S. Dubin, R. B. Kaner, K. Kalantar-Zadeh and W. Wlodarski, *J. Phys. Chem. C*, 2010, **114**, 13796.
19 S. Mao, S. M. Cui, G. H. Lu, K. H. Yu, Z. H. Wen and J. H. Chen, *J. Mater. Chem.*, 2012, **22**, 11009.
20 M. Gautam and A. H. Jayatissa, *J. Appl. Phys.*, 2012, **111**, 094317.
21 J. L. Johnson, A. Behnam, S. J. Pearton and A. Ural, *Adv. Mater.*, 2010, **22**, 4877.
22 Q. W. Huang, D. W. Zeng, H. Y. Li and C. S. Xie, *Nanoscale*, 2012, **4**, 5651.
23 M. Batzill and U. Diebold, *Prog. Surf. Sci.*, 2005, **79**, 47.
24 M. Batzill, *Sensors*, 2006, **6**, 1345.
25 Q. H. Wu, J. Li and S. G. Sun, *Curr. Nanosci.*, 2010, **6**, 525.
26 C. N. Xu, J. Tamaki, N. Miura and N. Yamazoe, *Sens. Actuators, B*, 1991, **3**, 147.
27 Y. D. Wang, I. Djerdj, M. Antonietti and B. Smarsly, *Small*, 2008, **4**, 1656.
28 D. Fattakhova-Rohfing, T. Brezesinski, J. Rathousky, A. Feldhoff, T. Oekermann, M. Wark and B. Smarsly, *Adv. Mater.*, 2006, **18**, 2980.
29 Y. D. Wang, T. Brezesinski, M. Antonietti and B. Smarsly, *ACS Nano*, 2009, **3**, 1373.
30 M. V. Vaishampayan, R. G. Deshmukh, P. Walke and I. S. Mulla, *Mater. Chem. Phys.*, 2008, **109**, 230.
31 M. Acciarri, R. Barberini, C. Canevali, M. Mattoni, C. M. Mari, F. Morazzoni, L. Nodari, S. Polizzi, R. Ruffo, U. Russo, M. Sala and R. Scotti, *Chem. Mater.*, 2005, **17**, 6167.
32 F. Pourfayaz, A. Khodadadi, Y. Mortazavi and S. S. Mohajerzadeh, *Sens. Actuators, B*, 2005, **108**, 172.
33 J. K. Choi, I. S. Hwang, S. J. Kim, J. S. Park, S. S. Park, U. Jeong, Y. C. Kang and J. H. Lee, *Sens. Actuators, B*, 2010, **150**, 191.
34 J. M. Samet, *Inhalation Toxicol.*, 2007, **19**, 1021.
35 B. Brunekreef and S. T. Holgate, *Lancet*, 2002, **360**, 1233.
36 J. Kaur, R. Kumar and M. C. Bhatnagar, *Sens. Actuators, B*, 2007, **126**, 478.
37 N. S. Ramgir, I. S. Mulla and K. P. Vijayamohanan, *Sens. Actuators, B*, 2005, **107**, 708.
38 S. Mao, K. H. Yu, S. M. Cui, Z. Bo, G. H. Lu and J. H. Chen, *Nanoscale*, 2011, **3**, 2849.
39 W. Hume-Rothery, *The structure of metals and alloys*, Institute of Metals, London, 1969.
40 Y. Shigesato, Y. Hayashi and T. Haranoh, *Appl. Phys. Lett.*, 1992, **61**, 73.
41 N. S. Ramgir, Y. K. Hwang, I. S. Mulla and J. S. Chang, *Solid State Sci.*, 2006, **8**, 359.
42 P. Nguyen, H. T. Ng, J. Kong, A. M. Cassell, R. Quinn, J. Li, J. Han, M. McNeil and M. Meyyappan, *Nano Lett.*, 2003, **3**, 925.
43 L. S. Zhang, L. Y. Jiang, H. J. Yan, W. D. Wang, W. Wang, W. G. Song, Y. G. Guo and L. J. Wan, *J. Mater. Chem.*, 2010, **20**, 5462.
44 K. N. Kudin, B. Ozbas, H. C. Schniepp, R. K. Prud'homme, I. A. Aksay and R. Car, *Nano Lett.*, 2008, **8**, 36.
45 S. Stankovich, D. A. Dikin, R. D. Piner, K. A. Kohlhaas, A. Kleinhammes, Y. Jia, Y. Wu, S. T. Nguyen and R. S. Ruoff, *Carbon*, 2007, **45**, 1558.
46 C. H. Xu, J. Sun and L. Gao, *Nanoscale*, 2012, **4**, 5425.
47 M. Zhang, D. Lei, Z. F. Du, X. M. Yin, L. B. Chen, Q. H. Li, Y. G. Wang and T. H. Wang, *J. Mater. Chem.*, 2011, **21**, 1673.
48 S. Cui, H. Pu, E. C. Mattson, G. Lu, S. Mao, M. Weinert, C. J. Hirschmugl, M. Gajdardziska-Josifovska and J. Chen, *Nanoscale*, 2012, **4**, 5887.
49 B. Slater, C. R. A. Catlow, D. E. Williams and A. M. Stoneham, *Chem. Commun.*, 2000, 1235.
50 Q. Wan and T. H. Wang, *Chem. Commun.*, 2005, 3841.
51 S. Srivastava, K. Jain, V. N. Singh, S. Singh, N. Vijayan, N. Dilawar, G. Gupta and T. D. Senguttuvan, *Nanotechnology*, 2012, **23**, 205501.
52 S. Deng, V. Tjoa, H. M. Fan, H. R. Tan, D. C. Sayle, M. Olivo, S. Mhaisalkar, J. Wei and C. H. Sow, *J. Am. Chem. Soc.*, 2012, **134**, 4905.
53 D. H. Zhang, Z. Q. Liu, C. Li, T. Tang, X. L. Liu, S. Han, B. Lei and C. W. Zhou, *Nano Lett.*, 2004, **4**, 1919.